PHYSICAL REVIEW B **109**, 014426 (2024)

Editors' Suggestion

Quantum magnetism in the frustrated square lattice oxyhalides $YbBi_2IO_4$ and $YbBi_2ClO_4$

Pyeongjae Park,[1,*] G. Sala,[2] Th. Proffen,[3] Matthew B. Stone,[3] Andrew D. Christianson,[1] and Andrew F. May[1,†]
[1]*Materials Science & Technology Division, Oak Ridge National Laboratory, Oak Ridge, Tennessee 37831, USA*
[2]*Spallation Neutron Source, Second Target Station, Oak Ridge National Laboratory, Oak Ridge, Tennessee 37831, USA*
[3]*Neutron Scattering Division, Oak Ridge National Laboratory, Oak Ridge, Tennessee 37831, USA*

(Received 21 November 2023; accepted 11 January 2024; published 25 January 2024)

Square-lattice systems offer a direct route for realizing two-dimensional (2D) quantum magnetism with frustration induced by competing interactions. In this work, the square lattice materials $YbBi_2IO_4$ and $YbBi_2ClO_4$ were investigated using a combination of magnetization and specific-heat measurements on polycrystalline samples. Specific-heat measurements provide evidence for long-range magnetic order below $T_N = 0.21$ K (0.25 K) for $YbBi_2IO_4$ ($YbBi_2ClO_4$). On the other hand, a rather broad maximum is found in the temperature-dependent magnetic susceptibility, located at $T_{max} = 0.33$ K (0.38 K) in $YbBi_2IO_4$ ($YbBi_2ClO_4$), consistent with the quasi-2D magnetism expected for the large separation between the magnetic layers. Estimation of the magnetic entropy supports the expected Kramers' doublet ground state for Yb^{3+} and the observed paramagnetic behavior is consistent with a well-isolated doublet. Roughly two-thirds of the entropy is consumed above T_N, due to a combination of the quasi-2D behavior and magnetic frustration. The impact of frustration is examined from the viewpoint of a simplified $J_1 - J_2$ square lattice model, which is frustrated for antiferromagnetic interactions. Specifically, a high-temperature series expansion analysis of the temperature-dependent specific-heat and magnetization data yields $J_2/J_1 = 0.30$ (=0.23) for $YbBi_2IO_4$ ($YbBi_2ClO_4$). This simplified analysis suggests strong frustration that should promote significant quantum fluctuations in these compounds, and thus motivates future work on the static and dynamic magnetic properties of these materials.

DOI: 10.1103/PhysRevB.109.014426

I. INTRODUCTION

The $S = 1/2$ square lattice antiferromagnet has served as a pivotal spin model for understanding quantum magnetism in two dimensions (2D) [1–5]. Intense interest in this model emerged from its relevance to high-temperature superconducting cuprates, in which the Cu^{2+} ions form a quasi-2D square lattice structure of spin-1/2 moments [1,6]. It was proposed that the inherent quantum spin fluctuations within this spin system contribute to the formation of superconductivity in cuprates. This was naturally extended to the suggestion of a new quantum-entangled magnetic ground state devoid of classical long-range order [7], now called a quantum spin liquid (QSL). Although it is now established that a $S = 1/2$ square lattice with nearest-neighbor (NN) antiferromagnetic interactions (J_1) develops long-range order, quantum fluctuations still play a role in this system [1,8–10]. This is notably evident through a large reduction in its ordered moment, which diminishes to approximately 60% of the classical limit [1,8]. Additionally, spectroscopic studies of the spin dynamics of $S = 1/2$ square lattice materials have revealed indications of fractionalized quasiparticles [9] and quantum entanglement [10], making model systems in this class potential testing grounds for such behavior.

The importance of quantum effects in $S = 1/2$ square lattice antiferromagnets can be further amplified by adding frustration. This can be realized by antiferromagnetic second-NN interactions (J_2). In this case, competition between J_1 and J_2 introduces exchange frustration on a square lattice, which, combined with low spin and low dimension, substantially increases the influence of quantum fluctuations [1–5]. In accordance with this idea, theoretical works have suggested the possible emergence of a QSL within a parameter range of $0.4 < J_2/J_1 < 0.6$ in which the frustration is maximized [11–14]. Notably, this phase emerges between the regions of Neel-type ($J_2/J_1 < 0.4$) and columnar-type ($0.6 < J_2/J_1$) antiferromagnetic orders, effectively bridging these two phases seamlessly by suppressing each order. Thus, the $S = 1/2$ J_1–J_2 square lattice model provides a simple but informative platform for studying 2D quantum magnetism where the degree of quantum fluctuations is systematically controlled by J_2. Consequently, continuous efforts have been made to find such frustrated $S = 1/2$ square lattice materials with sizable antiferromagnetic J_2 [15–19].

Halide-based materials have risen as important sources for studying magnetic behavior in 2D lattices [20]. Such investigations range from studying genuine 2D magnetism in atomically thin samples fabricated by mechanical exfoliation [21–25] to nearly ideal realizations of quantum magnetism [26–29]. Notably, the latter realizations were all achieved by spin-orbit-coupled electron configurations (i.e., J manifold) in which the Kramers' doublet ground states manifest an effective spin-1/2 ($J_{eff} = 1/2$) degree of

---

[*] parkp@ornl.gov
[†] mayaf@ornl.gov

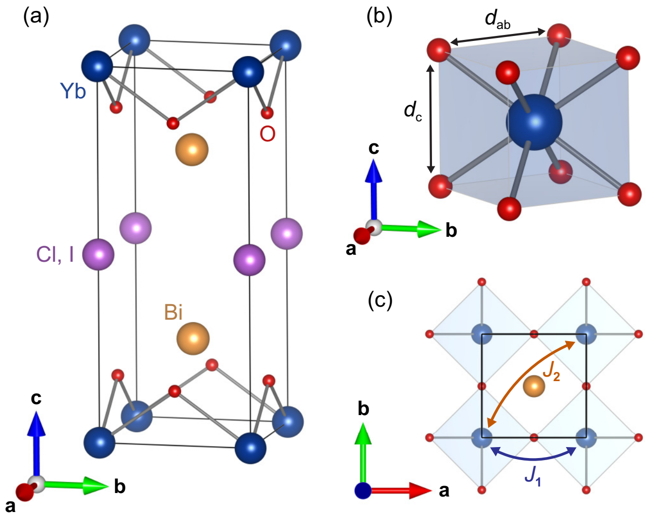

FIG. 1. Crystal structure of $YbBi_2XO_4$ (X=Cl, I). (a) The tetragonal unit cell of $YbBi_2XO_4$, having the space group $P4/mmm$ (No. 123). The Yb ions form a stack of square lattices separated by Bi and Cl (I) layers. (b) The oxygen coordination of the Yb ions. The distances between Yb and O are all equal. The ratio of in-plane to out-of-plane O-O distances (d_{ab}/d_c) are 0.996 for both $YbBi_2IO_4$ and $YbBi_2ClO_4$. (c) Nearest-neighbor (J_1) and second-nearest-neighbor (J_2) exchange interactions of a Yb^{3+} square lattice. Crystal structures were drawn with VESTA [31].

freedom. This pseudospin mechanism has provided an important method to design quantum magnets beyond cuprate (Cu^{2+}) or vanadate (V^{4+}) systems that have been the subjects of intense investigation [30]. Particular success has been found in hexagonal systems such as honeycomb $RuCl_3$ [26,27] and $YbCl_3$ [28], and triangular CoI_2 [29]. However, $J_{\mathrm{eff}} = 1/2$ square lattice materials built upon halide chemistry are still lacking.

In this article, we report the physical properties of the tetragonal materials $YbBi_2IO_4$ and $YbBi_2ClO_4$ (Fig. 1), which are members of a large class of oxyhalide magnetic materials $ReBi_2XO_4$ (Re = rare-earth elements, X = Cl, Br, I) [32]. The Yb sites in these compounds form square lattices, with the separation between each layer more than twice as long as the nearest Yb-Yb distance. The temperature-dependent magnetization precisely follows the Curie-Weiss behavior from 50 to ~1 K, with a negative Curie-Weiss temperature of $\theta_{\mathrm{CW}} = -0.78$ K (-0.73 K) in $YbBi_2IO_4$ ($YbBi_2ClO_4$). The specific-heat (C_p) measurements reveal the ordering of Yb^{3+} moments below $T_N = 0.21$ K (0.25 K) in $YbBi_2IO_4$ ($YbBi_2ClO_4$). The estimated total magnetic entropy [$\sim R\ln(2)$] indicates that Yb^{3+} in $YbBi_2IO_4$ and $YbBi_2ClO_4$ manifests well-isolated Kramers' doublet ground states, consistent with the Curie-Weiss law being valid up to 50 K $\sim 220\, T_N$. Meanwhile, temperature-dependent magnetic susceptibilities exhibit rather broad maxima at temperatures ($T_{\max}$) higher than T_N. This evidences strong spin correlations above T_N, consistent with the observation that the majority of the magnetic entropy is released above T_N in these materials. Notably, both the $|\theta_{\mathrm{CW}}|/T_{\max}$ ratio and J_2/J_1 estimated from a high-temperature series expansion analysis suggest these compounds possess sizable frustration, indicating a possibility of strong quantum effects.

II. EXPERIMENTAL DETAILS

Polycrystalline $YbBi_2IO_4$ and $YbBi_2ClO_4$ were formed by reactions of Bi_2O_3, Yb_2O_3, and BiIO or BiClO in evacuated SiO_2 tubing. $YbBi_2IO_4$ was obtained from a stoichiometric reaction at 950 °C for a total of 6 d with one intermediate grinding. For $YbBi_2ClO_4$, after an initial reaction at 950 °C for 100 h, the material was ground and heated at 900 °C for 100 h. After this, impurities were detected by laboratory x-ray diffraction, and thus an additional ≈1% of the original mass of BiClO and Bi_2O_3 was added and the sample was heated at 850 °C for 150 h, which resulted in the product used in the experiments reported herein. Yb_2O_3 was dried prior to use. The source powders of BiIO and BiClO were formed by reacting stoichiometric mixtures of Bi_2O_3 and ultradry BiI_3 spheres or anhydrous $BiCl_3$ at 550 °C for 24 h with an intermediate dwell of 10 h at 300–350 °C; the reagents were ground together in a glovebox and subsequently sealed under vacuum in SiO_2 without exposure to air.

Sample quality was initially checked using a commercial powder x-ray diffractometer (PANalytical X'Pert Pro MPD) with Cu–$K_{\alpha 1}$ radiation ($\lambda = 1.5406$ Å) from an incident beam monochromator. A full structural analysis was performed using neutron diffraction data collected at the POWGEN time-of-flight diffractometer at the Spallation Neutron Source (SNS) [33]. For the measurements, a $YbBi_2IO_4$ ($YbBi_2ClO_4$) powder sample with a mass of 6.09 g (3.73 g) was loaded in a standard vanadium can. The data were collected at 30 K with the high-resolution mode and a center wavelength of 1.5 Å. Rietveld refinement was performed using the FULLPROF software package [34].

Magnetization and specific-heat measurements were performed in Quantum Design measurement systems. Magnetization measurements were performed in an MPMS3 using a gelcap to hold the polycrystalline materials within a standard measurement straw. Data below 1.8 K were obtained using the iHe-3 insert, for which samples were affixed to the straw by mixing them with high-vacuum grease. Specific-heat measurements below 2.5 K were conducted using a dilution refrigerator insert within a Dynacool. In order to improve the mechanical integrity and thermal equilibration of the samples, the powders were gently ground with an equal mass of high-purity silver powder and then pressed into a small pellet. The contribution of the silver powder was subtracted using in-house data for silver's specific heat, which is much smaller than the magnetic contribution of the samples at low temperatures. AC susceptibility measurements down to 100 mK were performed using a dilution refrigerator insert with the ac-dr option from Quantum Design. A portion of the pellets used for specific heat (including Ag powder) was affixed to the sample holder using N-grease. Measurements were completed upon warming after thermalizing below 100 mK for several hours. Data were collected using 227 and 756 Hz and the broad maxima of susceptibility observed occurred at the same temperature for both frequencies; a static dc field was not applied and the ac driving amplitude was 2 Oe.

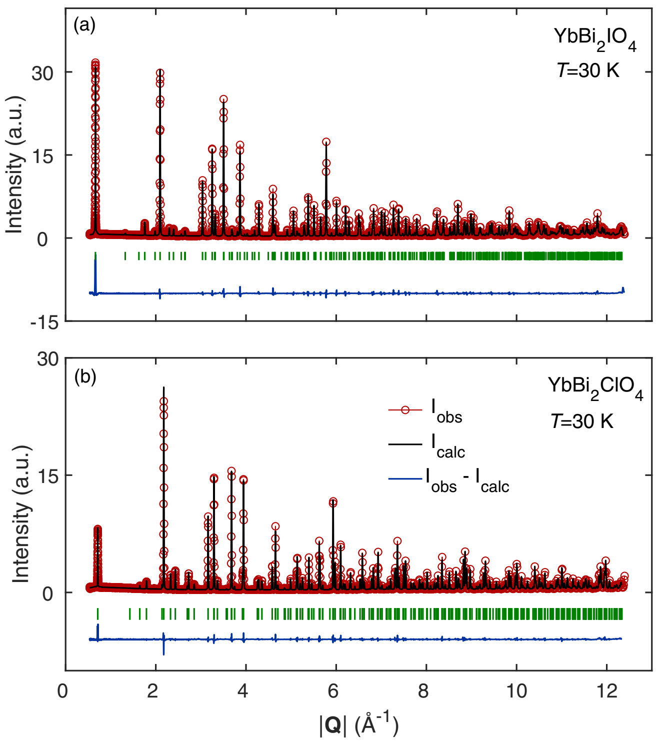

FIG. 2. Powder neutron diffraction profiles of (a) $YbBi_2IO_4$ and (b) $YbBi_2ClO_4$ collected at 30 K. Solid black lines in (a) and (b) are the simulated profile from the Rietveld refinement results shown in Table I. Solid blue lines are the difference between the data and simulations. Green vertical ticks denote the positions of nuclear reflections.

III. RESULTS

A. Structure analysis

The crystal structures of $YbBi_2IO_4$ and $YbBi_2ClO_4$ were studied through their time-of-flight neutron diffraction profiles collected at $T = 30$ K. Figure 2 shows the data and Rietveld refinement results as a function of momentum transfer $|\mathbf{Q}|$. Nuclear Bragg peaks of likely impurity phases [Yb_2O_3, YbI_2, BiI_3, Bi_2O_3, BiIO, $Yb(IO_3)_3$, $YbBi_2$, and Yb_5Bi_3] were not observed in the neutron diffraction profile. Yet we note that we observed two unidentified impurity peaks in the $YbBi_2IO_4$ data, located at $d = 1.84$ and 2.13 Å, with intensities less than 0.1% compared to those originating from $YbBi_2IO_4$. The refinements based on the previously reported tetragonal unit cell ($P4/mmm$) [32] yield an excellent agreement with the data, the results of which are summarized in Table I. Notably, the chloride exhibits smaller thermal displacement parameters (B_{iso}) of Yb, Bi, and O, which is especially noticeable on the Bi site.

The magnetic Yb^{3+} ions form a square lattice through edge sharing of square prismatic polyhedra, as shown in Figs. 1(b) and 1(c). The NN distances are equal to the a lattice parameter, and the second NN is on the diagonal at a distance of $\sqrt{2}a$. Each layer of the Yb^{3+} square lattice is well isolated from each other, with a separation equal to the c lattice parameter. As shown in Table I, the ratio of in-plane to out-of-plane distances is greater than 2 ($c/a = 2.308$ in $YbBi_2ClO_4$ and $c/a = 2.459$ in $YbBi_2IO_4$), which drives the expectation for genuine quasi-2D magnetic behavior dominated by square lattice physics. This remains true even when comparing the out-of-plane distance with the second-NN distance. The ratio ($c/\sqrt{2}a = 1.632$ in $YbBi_2ClO_4$ and 1.739 in $YbBi_2IO_4$) is still comparable or even larger than the ratio of in-plane to out-of-plane bond distances in other quasi-2D square lattice antiferromagnets [16,18,35,36]. Notably, the lattice parameter c of $YbBi_2IO_4$ is nearly 8% larger than that of $YbBi_2ClO_4$, while in-plane lattice parameters differ by ~1.2%, with the chloride having the smaller unit cell.

As expected from the space group, the oxygen coordination around Yb^{3+} is highly symmetric [Fig. 1(b)]. The eight O^{2-} ligands are evenly spaced from Yb^{3+} and form a nearly cubic-shaped polyhedron. Notably, the refined crystal structure of both $YbBi_2IO_4$ and $YbBi_2ClO_4$ possesses a slight (~0.4%) elongation of the polyhedron along the c axis, as evident from the ratio of in-plane to out-of-plane O-O distances ($d_{\text{ab}}/d_{\text{c}}$) being smaller than 1 [Fig. 1(b)].

B. Magnetization and heat-capacity measurements

Figures 3(a) and 3(b) show the temperature-dependent magnetization of $YbBi_2IO_4$ and $YbBi_2ClO_4$ from 50 to 0.4 K. Remarkably, $YbBi_2IO_4$ and $YbBi_2ClO_4$ exhibit almost the same magnetization curve. No sign of a phase transition is found in this temperature range. As evident from the inset of Fig. 3(a), the measured magnetization precisely follows the Curie-Weiss law for $2 < T < 50$ K. This implies that the excited crystal field levels of Yb^{3+} have a negligible contribution to the magnetism below 50 K. Orange

TABLE I. Crystal structure of $YbBi_2(I,Cl)O_4$ determined by Rietveld refinement of the powder neutron diffraction data collected at 30 K (Fig. 2). The space group is $P4/mmm$ (No. 123). The occupancies of all sites are equal to unity.

		$YbBi_2IO_4$ $a = b = 3.8658(1)$ Å, $c = 9.5052(1)$ Å				$YbBi_2ClO_4$ $a = b = 3.8196(1)$ Å, $c = 8.8169(1)$ Å			
Atom	Site	x/a	y/b	z/c	B_{iso} (Å^2)	x/a	y/b	z/c	B_{iso} (Å^2)
Yb	1a	0	0	0	0.057(14)	0	0	0	0.041(10)
(I,Cl)	1b	0	0	0.5	0.148(27)	0	0	0.5	0.235(13)
Bi	2h	0.5	0.5	0.7425(1)	0.038(10)	0.5	0.5	0.7195(1)	0.002(11)
O	4i	0.5	0	0.8581(1)	0.236(10)	0.5	0	0.8463(1)	0.193(12)
		$R_p(\%) = 8.26$, $R_{wp}(\%) = 6.86$ $R_{\text{exp}}(\%) = 0.722$, $\chi^2 = 90.4$				$R_p(\%) = 5.23$, $R_{wp}(\%) = 5.85$ $R_{\text{exp}}(\%) = 0.793$, $\chi^2 = 54.4$			

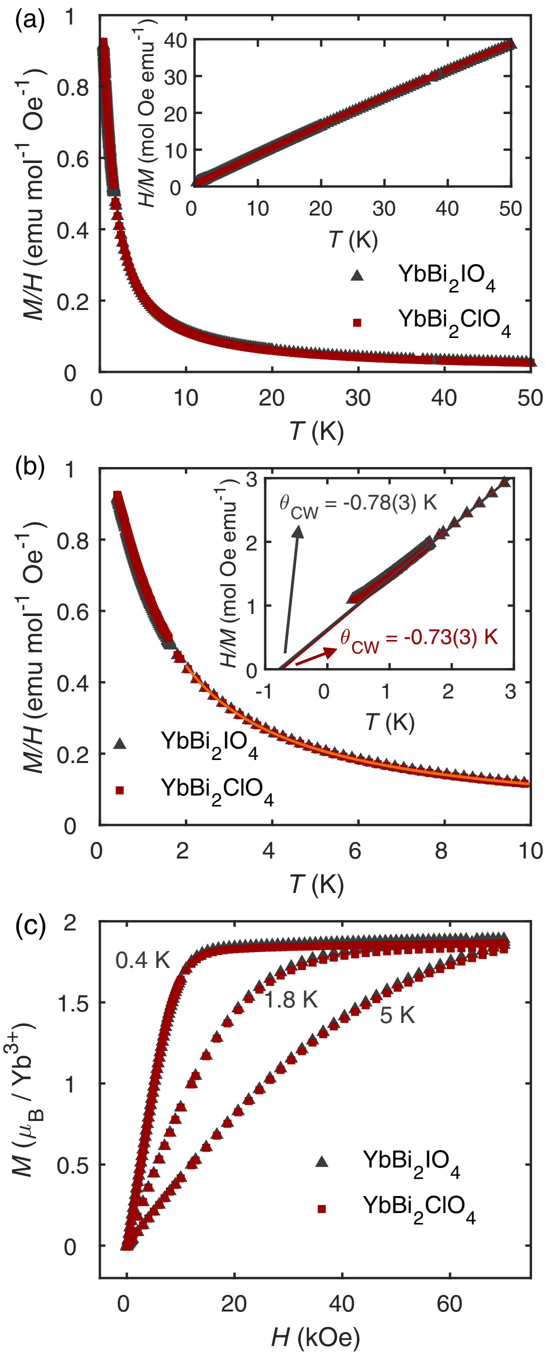

FIG. 3. Magnetic properties of YbBi$_2$IO$_4$ and YbBi$_2$ClO$_4$ above 0.4 K ($T > T_N$). (a),(b) Temperature-dependent magnetization data measured down to 0.4 K under a 10 kOe external magnetic field. The insets show the inverse magnetic susceptibility, demonstrating (a) the Curie-Weiss behavior below 50 K and (b) deviation from the Curie-Weiss behavior below around 0.8 K. Solids lines in (b) are fit to the modified Curie-Weiss law between 2 and 20 K. (b) Isothermal magnetization data from combined ^{3}He and ^{4}He experiments.

solid lines in Fig. 3(b) are the fit results with modified Curie-Weiss law [$\chi(T) = \chi_0 + C/(T - \theta_{CW})$, where θ_{CW} denotes the Curie-Weiss temperature] for a temperature range from 2 to 20 K. The fitting yielded $\theta_{CW} = -0.78(3)$ K and $\mu_{eff} = 3.15(1)\mu_B$ for YbBi$_2$IO$_4$, and $\theta_{CW} = -0.73(3)$ K and $\mu_{eff} = 3.12(1)$ μ_B for YbBi$_2$ClO$_4$. Note that the fitted χ_0 was less than 10^{-3} emu mol^{-1} Oe^{-1} for both compounds. As expected from the magnitude of fitted θ_{CW}, the measured M/H deviates from the Curie-Weiss behavior below around 0.8 K; see the inset of Fig. 3(b).

The isothermal magnetization data shown in Fig. 3(c) provide further information of the Yb^{3+} magnetism in YbBi$_2$IO$_4$ and YbBi$_2$ClO$_4$. At 0.4 K, full polarization of magnetic moments is achieved by applying a magnetic field up to 70 kOe. The saturated magnetization estimated from the high-field data yields $\sim$1.8 μ_B/Yb^{3+} for each compound. For $J_{eff} = 1/2$ (as will become clear in the following paragraphs), this indicates the averaged g factor of $\sim$3.6 for each compound, which is consistent with the magnitude of $\mu_{eff} = g\sqrt{J(J+1)}$ ($J = 1/2$) obtained from the Curie-Weiss fitting assumed to occur within the doublet.

Upon further cooling, we observed clear signs of magnetic phase transitions in YbBi$_2$IO$_4$ and YbBi$_2$ClO$_4$. First, a broad peak appears in the real part of the ac magnetic susceptibility (χ'_{ac}) measured down to $\sim$0.1 K in a dilution refrigerator [Fig. 4(a)]. This peak is centered at $T_{max} = 0.33$ K for YbBi$_2$IO$_4$ and $T_{max} = 0.38$ K for YbBi$_2$ClO$_4$. This behavior is associated with short-range correlations above T_N due to the 2D character of the magnetism. In addition, no meaningful signal was found in the imaginary part (χ''_{ac}), implying a fully compensated antiferromagnetic spin structure (i.e., zero net magnetization) of YbBi$_2$IO$_4$ and YbBi$_2$ClO$_4$ [37].

On the other hand, the heat-capacity measurements are characterized by a sharp λ-shaped peak at 0.21 K (0.25 K) for YbBi$_2$IO$_4$ (YbBi$_2$ClO$_4$), which suggests the onset of long-range order in these compounds [Fig. 4(b)]. These transition temperatures (T_N) are $\sim$1.54 times lower than T_{max} found in the ac susceptibility. Notably, the T_N of YbBi$_2$ClO$_4$ is 19% higher than that of YbBi$_2$IO$_4$, consistent with the observation that T_{max} was 15% higher in YbBi$_2$ClO$_4$.

The magnetic entropy across the phase transition was estimated by integrating C_p/T and the results are shown in Fig. 4(c). Due to the very low temperatures involved, the phonon contribution to the entropy is assumed to be negligible in Fig. 4(c). The entropy saturates to $\approx R\ln(2)$ ($R = 8.314$ J K^{-1}mol^{-1}), suggesting a well-isolated Kramers' doublet ground state that gives rise to $J_{eff} = 1/2$ magnetic moments. This isolation is also evident in the fact that both YbBi$_2$IO$_4$ and YbBi$_2$ClO$_4$ follow the Curie-Weiss law up to 50 K ($\sim$220 T_N); thermal populations of higher-energy crystal field levels should be nearly zero around a few kelvin. In addition to supporting the $J_{eff} = 1/2$ picture in these compounds, the entropy calculation reveals that nearly two-thirds of the total magnetic entropy is consumed above T_N. This indicates the formation of sizable spin-spin correlation at a temperature that is 3–4 times higher than T_N, consistent with the deviation from the Curie-Weiss behavior below 0.8 K [Fig. 3(a)].

IV. DISCUSSION

The size of θ_{CW}, T_{max}, and T_N in YbBi$_2$IO$_4$ and YbBi$_2$ClO$_4$ merits a deeper quantitative comparison as a diagnostic of whether these systems are frustrated. This is because T_{max} and T_N are suppressed by frustration, whereas θ_{CW} simply captures a sum of all exchange interactions in a spin

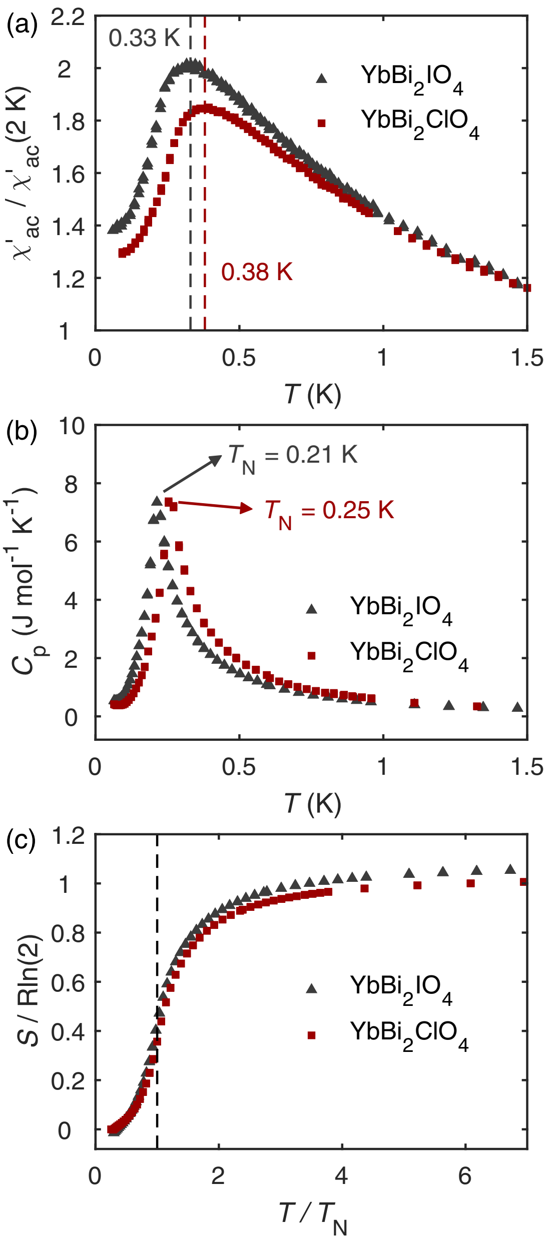

FIG. 4. Phase transitions and magnetic correlations found for $T < 0.4$ K. (a) Temperature-dependent ac susceptibility (f = 756 Hz) measured down to 100 mK. (b) Heat capacity (C_P) of YbBi$_2$IO$_4$ and YbBi$_2$ClO$_4$ around their Neel temperatures T_N = 0.21 and 0.25 K, respectively. (c) The entropy obtained by direct integration of measured C_P/T without any background subtraction.

system [i.e., $\theta_{CW} \propto (J_1 + J_2)$ for the J_1–J_2 model]. First, even though the ratio $|\theta_{CW}|/T_N = 3.71$ (= 2.92) found in YbBi$_2$IO$_4$ (YbBi$_2$ClO$_4$) largely surpasses 1, this alone should not be deemed as an indication of frustration in a 2D square lattice antiferromagnet. This is because T_N also depends on the size of the interlayer coupling (J_c) and thus $|\theta_{CW}|/T_N$ larger than 1 can occur without any frustration. Previous experimental studies of quasi-2D square lattice antiferromagnets demonstrate such a case: while they reported $|\theta_{CW}|/T_N \sim 2.75$ for Sr$_2$CuTeO$_6$ and $|\theta_{CW}|/T_N \sim 1.7$ for Zn$_2$VO(PO$_4$)$_2$, both compounds are known to have very small J_2/J_1 (i.e., very little frustration) [17,36].

Instead, $|\theta_{CW}|/T_{max}$ better estimates the degree of frustration as T_{max} stems from the spin correlation of a 2D square lattice. Indeed, this ratio was reported to be close to 1 for both Sr$_2$CuTeO$_6$ and Zn$_2$VO(PO$_4$)$_2$ [17,36], and quantum Monte Carlo simulations yield $|\theta_{CW}|/T_{max} = 1.069$ (close to 1) for $J_2 = 0$ in the J_1–J_2 model [16,38]. Interestingly, the $|\theta_{CW}|/T_{max}$ values of YbBi$_2$IO$_4$ and YbBi$_2$ClO$_4$ are 2.36 and 1.92, respectively, suggesting both YbBi$_2$IO$_4$ and YbBi$_2$ClO$_4$ possess frustration. This frustration, in addition to the pronounced 2D character, may have further contributed to the significant spin-spin correlations above T_N in YbBi$_2$(I,Cl)O$_4$. However, it is important to note that a fitted θ_{CW} value can be influenced by various extrinsic factors in the measurement, necessitating more concrete evidence of frustration in YbBi$_2$IO$_4$ and YbBi$_2$ClO$_4$.

To further explore the possibility of frustrated interactions, we conducted a high-temperature series expansion analysis based on the $S = 1/2$ J_1–J_2 Heisenberg model frequently used for frustrated square lattices. This was done by performing a dual fit of measured $C_p(T)$ and $\chi(T)$ with their theoretical form derived by the high-temperature series expansion. We assumed J_1 is larger than J_2 as is more likely from a bond length perspective. The resultant J_1 and J_2 values enable us to estimate the degree of frustration for each compound based on J_2/J_1. We used the analytic forms derived by Ref. [39] that include polynomials up to the eighth order. The temperature range for the fitting was set to $0.6 < T < 4$ K for C_p; the magnetic contribution above 4 K is nearly zero and the lattice contribution is negligible below 4 K. For $\chi(T)$, we used $0.6 < T < 10$ K. Note that the high-temperature series expansion is valid only for a temperature range higher than the thermodynamic energy scale of a spin system, i.e., $k_BT > S(S+1)\sqrt{J_1{}^2 + J_2{}^2}$ [39]. As will become clear in the following paragraph, 0.6 K is much higher than the thermodynamic energy scale of YbBi$_2$IO$_4$ and YbBi$_2$ClO$_4$ obtained from this analysis, thereby satisfying the aforementioned condition. Calculated $C_p(T)$ and $\chi(T)$ were multiplied by scale factors to match their magnitude with our data [Figs. 5(a)–5(d)]. In other words, our analysis only fitted the temperature dependence of $C_p(T)$ and $\chi(T)$, which is sensitive enough to discern the optimal values of J_1 and J_2.

Before presenting the results of our series expansion analysis, we would like to briefly mention a potential impurity signal in $C_p(T)$ of YbBi$_2$IO$_4$ around 2.2 K [Fig. 5(a)]. The most likely impurity candidate is Yb$_2$O$_3$ as it undergoes a magnetic phase transition at 2.25 K [40]. However, as mentioned earlier in this article, our powder neutron diffraction data (Fig. 2) revealed no nuclear Bragg peaks of Yb$_2$O$_3$. This observation raises two possibilities: (i) the quantity of Yb$_2$O$_3$, though not negligible, might be exceedingly small, or (ii) it falls outside the range of considered impurity candidates, possibly related to the two unidentified impurity peaks found in our neutron diffraction data (see Sec. III A).

Figures 5(a)–5(d) display the optimal fit results for YbBi$_2$IO$_4$ and YbBi$_2$ClO$_4$, and corresponding parameters are marked as orange stars in Figs. 5(e) and 5(f): (J_1, J_2) = (0.043, 0.013 meV) for YbBi$_2$IO$_4$ and (0.043, 0.010 meV) for YbBi$_2$ClO$_4$. Regarding potential systematic errors included in

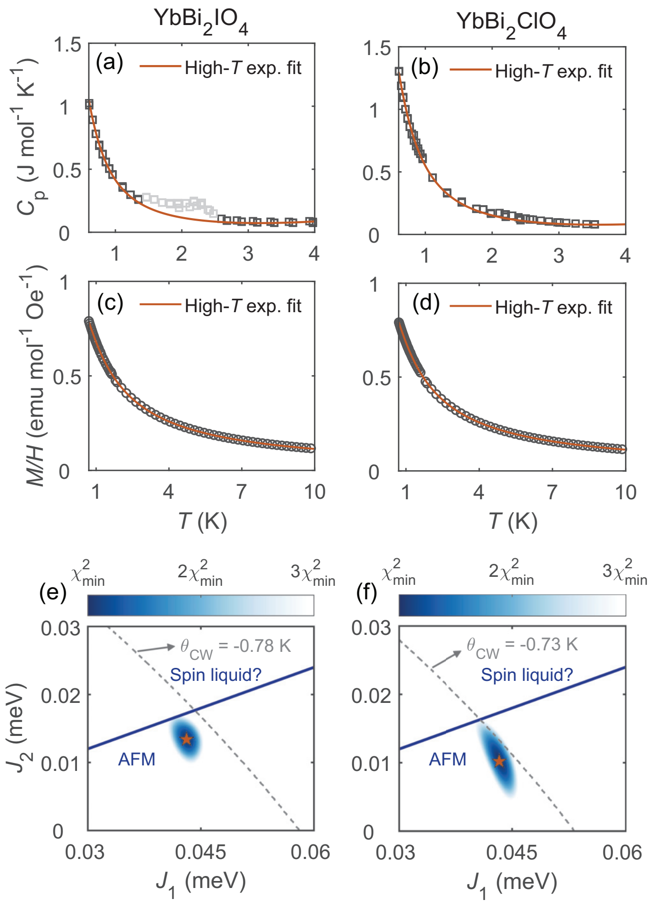

FIG. 5. Quantitative analysis of the first- and second-NN exchange interactions using a high-temperature series expansion methodology. [(a)–(d)] Best fit of the measured C_p and $\chi(T)$ with the high-temperature series expansion. The grayed data points in (a) contain a putative impurity signal and thus are excluded from the fitting. A short note on this impurity is provided in the main text. (e),(f) Two-dimensional color plots of the goodness-of-fit (χ^2) as a function of J_1 and J_2. Orange star symbols denote J_1 and J_2 of the best fits ($\chi^2 = \chi^2_{\rm min}$) shown in [(a)–(d)]. Blue solid lines in (e) and (f) are the boundary between the Neel-type antiferromagnetic order and the spin-liquid phase ($J_2 = 0.4J_1$). Gray dashed lines in (e) and (f) indicate the (J_1, J_2) parameter sets that yield $\theta_{\rm CW} = -0.78$ and -0.73 K in $\chi(T)$ of the high-temperature series expansion.

this analysis, the fitted parameters contain uncertainty to some extent, which are roughly represented by the blue-colored regions in Figs. 5(e) and 5(f). The range $0.26 \leqslant J_2/J_1 \leqslant 0.37$ ($0.16 \leqslant J_2/J_1 \leqslant 0.34$) expresses the uncertainty based on $2\chi^2_{\rm min}$ in YbBi$_2$IO$_4$ (YbBi$_2$ClO$_4$). However, even considering such uncertainty, our analysis clearly suggests sizable antiferromagnetic J_2 in both compounds, again indicating YbBi$_2$IO$_4$ and YbBi$_2$ClO$_4$ are frustrated. In addition, we varied the fitted temperature ranges and only observed small variations of J_1 and J_2 values within the uncertainty illustrated as the blue-colored regions in Figs. 5(e) and 5(f).

Another noteworthy result is that the fitted J_2/J_1 of YbBi$_2$IO$_4$ (∼0.30) is larger than that of YbBi$_2$ClO$_4$(∼0.23), implying that YbBi$_2$IO$_4$ possesses stronger frustration. This can naturally describe the lower $T_{\rm N}$ and $T_{\rm max}$ of YbBi$_2$IO$_4$ than those of YbBi$_2$ClO$_4$, despite its larger (or nearly equal) $|\theta_{\rm CW}|$. However, we note that qualitatively the same tendency can be mimicked if YbBi$_2$ClO$_4$ has stronger ferromagnetic J_c; this also increases $T_{\rm N}$ while decreasing $|\theta_{\rm CW}|$ to some extent. A shorter c lattice parameter found in YbBi$_2$ClO$_4$ (see Table I) further supports this possibility. Yet the sign of J_c cannot be determined by the results presented in this work. This requires a magnetic neutron diffraction measurement, which can confirm the sign of J_c by revealing relative spin alignment between the Yb^{3+} moments connected by J_c. Meanwhile, a comparison to exact-diagonalization (ED) results implies that our analysis might be underestimating J_2/J_1: according to ED, $|\theta_{\rm CW}|/T_{\rm max} = 1.92$ found in YbBi$_2$ClO$_4$ corresponds to J_2/J_1 larger than 0.25 [16]. Therefore, the accurate values of J_2/J_1, as well as the validity of the J_1–J_2 model, should be confirmed by future measurements (e.g., inelastic neutron scattering). In particular, symmetry-allowed anisotropic exchange interactions are another possible source of frustration, which are not considered in our isotropic spin model. Although recent studies suggest that Yb^{3+}-based quantum magnets often consist of Heisenberg-type exchange interactions [28,41], future inelastic neutron scattering experiments are required to clarify this possibility.

Based on the parameters suggested by the high-temperature series expansion analysis, both compounds lie in the region of a classical Neel-type magnetic ground state. However, they are very close to the highly frustrated regime in the $S = 1/2$ J_1–J_2 square lattice model. This is evident in Figs. 5(e) and 5(f); the fitted J_2/J_1 (especially for YbBi$_2$IO$_4$) are not far from the suggested phase boundary line between the Neel order and spin liquid ($J_2 = 0.4J_1$). Thus, sizable quantum fluctuations are expected in these compounds. For instance, in a $S = 1/2$ triangular lattice antiferromagnet, proximity to its spin-liquid region led to an observation of significant quantum entanglement between local moments and the dominance of fractionalized quasiparticles, even though a classical long-range order is present [41]. Similar exotic features might be anticipated in the highly frustrated $S = 1/2$ square lattice, thereby making YbBi$_2$IO$_4$ and YbBi$_2$ClO$_4$ worthy of further investigation.

V. CONCLUSION

We have studied the magnetic properties of YbBi$_2$IO$_4$ and YbBi$_2$ClO$_4$ by measuring their specific heat and magnetization. The results suggest that the Yb^{3+} sublattice realizes an ideal $J_{\rm eff} = 1/2$ square lattice by forming a well-isolated Kramers' doublet. The specific-heat measurements reveal that YbBi$_2$IO$_4$ and YbBi$_2$ClO$_4$ form long-range order below $T_{\rm N} = 0.21$ and 0.25 K, respectively. However, sizable spin correlations are evidenced at temperatures much higher than $T_{\rm N}$, which is attributed to a combination of pronounced two-dimensional character and frustration. YbBi$_2$IO$_4$ and YbBi$_2$ClO$_4$ could be ideal platforms for investigating the quantum effects of frustrated square lattice antiferromagnets, and thus this study motivates future work on the magnetic ground state and excitations in these and related phases.

ACKNOWLEDGMENTS

This research was supported by the U.S. Department of Energy, Office of Science, Basic Energy Sciences, Materials Science and Engineering Division. A portion of this research used resources at the Spallation Neutron Source, a DOE Office of Science User Facility operated by the Oak Ridge National Laboratory (ORNL). ORNL is managed by UT-Battelle, LLC under Contract No. DE-AC05-00OR22725 for the U.S. Department of Energy. The United States Government retains and the publisher, by accepting the article for publication, acknowledges that the United States Government retains a nonexclusive, paid-up, irrevocable, worldwide license to publish or reproduce the published form of this manuscript, or allow others to do so, for United States Government purposes.

---

[1] J. D. Reger and A. P. Young, Monte Carlo simulations of the spin-1/2 Heisenberg antiferromagnet on a square lattice, Phys. Rev. B **37**, 5978 (1988).

[2] E. Dagotto and A. Moreo, Phase diagram of the frustrated spin-1/2 Heisenberg antiferromagnet in two dimensions, Phys. Rev. Lett. **63**, 2148 (1989).

[3] M. S. Makivić and H.-Q. Ding, Two-dimensional spin-1/2 Heisenberg antiferromagnet: A quantum Monte Carlo study, Phys. Rev. B **43**, 3562 (1991).

[4] H. J. Schulz and T. A. L. Ziman, Finite-size scaling for the two-dimensional frustrated quantum Heisenberg antiferromagnet, Europhys. Lett. **18**, 355 (1992).

[5] P. Chandra and B. Doucot, Possible spin-liquid state at large S for the frustrated square Heisenberg lattice, Phys. Rev. B **38**, 9335 (1988).

[6] E. Manousakis, The spin-1/2 Heisenberg antiferromagnet on a square lattice and its application to the cuprous oxides, Rev. Mod. Phys. **63**, 1 (1991).

[7] P. W. Anderson, The resonating valence bond state in La_2CuO_4 and superconductivity, Science **235**, 1196 (1987).

[8] C. J. Hamer, Weihong Zheng, and P. Arndt, Third-order spin-wave theory for the Heisenberg antiferromagnet, Phys. Rev. B **46**, 6276 (1992).

[9] B. Dalla Piazza, M. Mourigal, N. B. Christensen, G. J. Nilsen, P. Tregenna-Piggott, T. G. Perring, M. Enderle, D. F. McMorrow, D. A. Ivanov, and H. M. Rønnow, Fractional excitations in the square-lattice quantum antiferromagnet, Nat. Phys. **11**, 62 (2015).

[10] N. B. Christensen, H. M. Rønnow, D. F. McMorrow, A. Harrison, T. G. Perring, M. Enderle, R. Coldea, L. P. Regnault, and G. Aeppli, Quantum dynamics and entanglement of spins on a square lattice, Proc. Natl. Acad. Sci. USA **104**, 15264 (2007).

[11] H.-C. Jiang, H. Yao, and L. Balents, Spin liquid ground state of the spin-$\frac{1}{2}$ square $J_1 - J_2$ Heisenberg model, Phys. Rev. B **86**, 024424 (2012).

[12] S. Morita, R. Kaneko, and M. Imada, Quantum spin liquid in spin 1/2 $J_1 - J_2$ Heisenberg model on square lattice: Many-variable variational Monte Carlo study combined with quantum-number projections, J. Phys. Soc. Jpn. **84**, 024720 (2015).

[13] S.-S. Gong, W. Zhu, D. N. Sheng, O. I. Motrunich, and M. P. A. Fisher, Plaquette ordered phase and quantum phase diagram in the spin $-\frac{1}{2}J_1 - J_2$ square Heisenberg model, Phys. Rev. Lett. **113**, 027201 (2014).

[14] W.-Y. Liu, S.-S. Gong, Y.-B. Li, D. Poilblanc, W.-Q. Chen, and Z.-C. Gu, Gapless quantum spin liquid and global phase diagram of the spin-1/2 $J_1 - J_2$ square antiferromagnetic Heisenberg model, Sci. Bull. **67**, 1034 (2022).

[15] P. Carretta, N. Papinutto, C. B. Azzoni, M. C. Mozzati, E. Pavarini, S. Gonthier, and P. Millet, Frustration-driven structural distortion in $VOMoO_4$, Phys. Rev. B **66**, 094420 (2002).

[16] R. Melzi, P. Carretta, A. Lascialfari, M. Mambrini, M. Troyer, P. Millet, and F. Mila, $Li_2VO(Si, Ge)O_4$, a prototype of a two-dimensional frustrated quantum Heisenberg antiferromagnet, Phys. Rev. Lett. **85**, 1318 (2000).

[17] O. Mustonen, S. Vasala, E. Sadrollahi, K. P. Schmidt, C. Baines, H. C. Walker, I. Terasaki, F. J. Litterst, E. Baggio-Saitovitch, and M. Karppinen, Spin-liquid-like state in a spin-1/2 square-lattice antiferromagnet perovskite induced by d^{10}–d^0 cation mixing, Nat. Commun. **9**, 1085 (2018).

[18] S. Vasala, J. G. Cheng, H. Yamauchi, J. B. Goodenough, and M. Karppinen, Synthesis and characterization of $Sr_2Cu(W_{1-x}Mo_x)O_6$: A quasi-two-dimensional magnetic system, Chem. Mater. **24**, 2764 (2012).

[19] M. Watanabe, N. Kurita, H. Tanaka, W. Ueno, K. Matsui, and T. Goto, Valence-bond-glass state with a singlet gap in the spin-$\frac{1}{2}$ square-lattice random $J_1 - J_2$ Heisenberg antiferromagnet $Sr_2CuTe_{1-x}W_xO_6$, Phys. Rev. B **98**, 054422 (2018).

[20] M. McGuire, Crystal and magnetic structures in layered, transition metal dihalides and trihalides, Crystals **7**, 121 (2017).

[21] B. Huang, G. Clark, E. Navarro-Moratalla, D. R. Klein, R. Cheng, K. L. Seyler, D. Zhong, E. Schmidgall, M. A. McGuire, and D. H. Cobden, Layer-dependent ferromagnetism in a van der Waals crystal down to the monolayer limit, Nature (London) **546**, 270 (2017).

[22] Q. Song, C. A. Occhialini, E. Ergeçen, B. Ilyas, D. Amoroso, P. Barone, J. Kapeghian, K. Watanabe, T. Taniguchi, and A. S. Botana, Evidence for a single-layer van der Waals multiferroic, Nature (London) **602**, 601 (2022).

[23] H. Ju, Y. Lee, K.-T. Kim, I. H. Choi, C. J. Roh, S. Son, P. Park, J. H. Kim, T. S. Jung, and J. H. Kim, Possible persistence of multiferroic order down to bilayer limit of van der Waals material NiI_2, Nano Lett. **21**, 5126 (2021).

[24] K. S. Burch, D. Mandrus, and J.-G. Park, Magnetism in two-dimensional van der Waals materials, Nature (London) **563**, 47 (2018).

[25] B. Huang, M. A. McGuire, A. F. May, D. Xiao, P. Jarillo-Herrero, and X. Xu, Emergent phenomena and proximity effects in two-dimensional magnets and heterostructures, Nat. Mater. **19**, 1276 (2020).

[26] A. Banerjee, J. Yan, J. Knolle, C. A. Bridges, M. B. Stone, M. D. Lumsden, D. G. Mandrus, D. A. Tennant, R. Moessner, and S. E. Nagler, Neutron scattering in the proximate quantum spin liquid $\alpha - RuCl_3$, Science **356**, 1055 (2017).

[27] S.-H. Do, S.-Y. Park, J. Yoshitake, J. Nasu, Y. Motome, Y. S. Kwon, D. Adroja, D. Voneshen, K. Kim, and T.-H. Jang, Majorana fermions in the Kitaev quantum spin system $\alpha - RuCl_3$, Nat. Phys. **13**, 1079 (2017).

[28] G. Sala, M. B. Stone, B. K. Rai, A. F. May, P. Laurell, V. O. Garlea, N. P. Butch, M. D. Lumsden, G. Ehlers, and G. Pokharel, Van hove singularity in the magnon spectrum of the antiferromagnetic quantum honeycomb lattice, Nat. Commun. **12**, 171 (2021).

[29] C. Kim, S. Kim, P. Park, T. Kim, J. Jeong, S. Ohira-Kawamura, N. Murai, K. Nakajima, A. Chernyshev, M. Mourigal *et al.*, Bond-dependent anisotropy and magnon decay in cobalt-based Kitaev triangular antiferromagnet, Nat. Phys. **19**, 1624 (2023).

[30] D. Inosov, Quantum magnetism in minerals, Adv. Phys. **67**, 149 (2018).

[31] K. Momma and F. Izumi, *VESTA3* for three-dimensional visualization of crystal, volumetric and morphology data, J. Appl. Crystallogr. **44**, 1272 (2011).

[32] M. Schmidt, H. Oppermann, C. Hennig, R. Henn, E. Gmelin, N. Söger, and M. Binnewies, Investigations on the bismuth rare-earth oxyhalides Bi_2REO_4X (X = Cl, Br, I), Z. Anorg. Allg. Chem. **626**, 125 (2000).

[33] A. Huq, J. P. Hodges, L. Heroux, and O. Gourdon, Powgen: A third-generation high resolution high-throughput powder diffraction instrument at the spallation neutron source, Z. Kristallogr. Proc. **1**, 127 (2011).

[34] J. Rodriguez-Carvajal, Recent advances in magnetic structure determination by neutron powder diffraction, Phys. B: Condens. Matter **192**, 55 (1993).

[35] O. Mustonen, S. Vasala, K. P. Schmidt, E. Sadrollahi, H. C. Walker, I. Terasaki, F. J. Litterst, E. Baggio-Saitovitch, and M. Karppinen, Tuning the $S = 1/2$ square-lattice antiferromagnet $Sr_2Cu(Te_{1-x}W_x)O_6$ from Néel order to quantum disorder to columnar order, Phys. Rev. B **98**, 064411 (2018).

[36] N. Kini, E. Kaul, and C. Geibel, $Zn_2VO(PO_4)_2$: an S= 1/2 Heisenberg antiferromagnetic square lattice system, J. Phys.: Condens. Matter **18**, 1303 (2006).

[37] M. Bałanda, AC susceptibility studies of phase transitions and magnetic relaxation: Conventional, molecular and low-dimensional magnets, Acta Phys. Pol. A **124**, 964 (2013).

[38] H. Kageyama, T. Kitano, N. Oba, M. Nishi, S. Nagai, K. Hirota, L. Viciu, W. JB, J. Yasuda, Y. Baba *et al.*, Spin-singlet ground state in two-dimensional $S = 1/2$ frustrated square lattice:$(CuCl)LaNb_2O_7$, J. Phys. Soc. Jpn. **74**, 1702 (2005).

[39] H.-J. Schmidt, A. Lohmann, and J. Richter, Eighth-order high-temperature expansion for general Heisenberg Hamiltonians, Phys. Rev. B **84**, 104443 (2011).

[40] R. Moon, H. Child, W. Koehler, and L. Raubenheimer, Magnetic structure of Er_2O_3 and Yb_2O_3, J. Appl. Phys. **38**, 1383 (1967).

[41] A. O. Scheie, E. A. Ghioldi, J. Xing, J. A. M. Paddison, N. E. Sherman, M. Dupont, L. D. Sanjeewa, Sangyun Lee, A. J. Woods, D. Abernathy *et al.*, Proximate spin liquid and fractionalization in the triangular antiferromagnet $KYbSe_2$, Nat. Phys. **20**, 74 (2024).